Stem Cell Reports
Article

ISSCR

OPEN ACCESS

A critical role of retinoic acid concentration for the induction of a fully human-like atrial action potential phenotype in hiPSC-CM

Carl Schulz,[1,2] Muhammed Sönmez,[1,2] Julia Krause,[1,2,3,6] Edzard Schwedhelm,[2,4] Pan Bangfen,[1,2] Dzenefa Alihodzic,[5] Arne Hansen,[1,2] Thomas Eschenhagen,[1,2,*] and Torsten Christ[1,2,*]

[1]Institute of Experimental Pharmacology and Toxicology, University Medical Center Hamburg-Eppendorf, Hamburg, Germany
[2]German Centre for Cardiovascular Research (DZHK), Partner Site Hamburg/Kiel/Lübeck, Hamburg, Germany
[3]Department of Cardiology, University Heart and Vascular Center, Hamburg, Germany
[4]Institute of Clinical Pharmacology and Toxicology, University Medical Center Hamburg-Eppendorf, Hamburg, Germany
[5]Hospital Pharmacy, University Medical Center Hamburg-Eppendorf, Hamburg, Germany
[6]Present address: Stem Cell Biology, Novo Nordisk A/S, Måløv, Denmark
*Correspondence: t.eschenhagen@uke.de (T.E.), t.christ@uke.de (T.C.)
https://doi.org/10.1016/j.stemcr.2023.10.006

SUMMARY

Retinoic acid (RA) induces an atrial phenotype in human induced pluripotent stem cells (hiPSCs), but expression of atrium-selective currents such as the ultrarapid (I_{Kur}) and acetylcholine-stimulated K^+ current is variable and less than in the adult human atrium. We suspected methodological issues and systematically investigated the concentration dependency of RA. RA treatment increased I_{Kur} concentration dependently from 1.1 ± 0.54 pA/pF (0 RA) to 3.8 ± 1.1, 5.8 ± 2.5, and 12.2 ± 4.3 at 0.01, 0.1, and 1 μM, respectively. Only 1 μM RA induced enough I_{Kur} to fully reproduce human atrial action potential (AP) shape and a robust shortening of APs upon carbachol. We found that sterile filtration caused substantial loss of RA. We conclude that 1 μM RA seems to be necessary and sufficient to induce a full atrial AP shape in hiPSC-CM in EHT format. RA concentrations are prone to methodological issues and may profoundly impact the success of atrial differentiation.

INTRODUCTION

Human induced pluripotent stem cell-derived cardiomyocytes (hiPSC-CMs) represent a model to study the electrophysiological consequences of gene variants and mutations on a human background. Consequently, several models have been developed to investigate ventricular arrhythmias. However, atrial fibrillation (AF) is much more common than ventricular arrhythmias and cannot yet be studied sufficiently in hiPSC-CM. Atrial-like hiPSC-CMs (hiPSC-aCM) resembling the electrophysiological properties of the human atrium could be used to investigate mechanisms of AF *in vitro*. In addition, hiPSC-aCMs could give fundamental insight into pacing-induced electrical remodeling, a technique frequently used in animals that lead to the widely accepted concept of AF-induced remodeling (Wijffels et al., 1995). Thus, recently developed protocols for the differentiation of hiPSC-aCM are an important progression in modeling atrial electrophysiology in a human setting (Goldfracht et al., 2020; Laksman et al., 2017; Soepriatna et al., 2021).

Retinoic acid (RA) has been identified as a critical factor during atrial differentiation of hiPSC (Devalla et al., 2015; Lee et al., 2017). Inclusion of RA in standard differentiation protocols induced several electrophysiological parameters indicating an atrial, rather than ventricular, phenotype of the resulting hiPSC-aCM. The presence of the G-protein-gated K^+ channel ($I_{K,ACh}$) is a hallmark of atrial and absent in ventricular CMs (Heidbüchel et al., 1987); therefore, researchers have looked for the shortening of the action potential duration at 90% repolarization (APD_{90}) upon activation of muscarinic receptors, but effect sizes were small and variable in two studies (Devalla et al., 2015; Lemme et al., 2018). Large mammals (dog and human) also possess large transient potassium currents consisting of the transient outward current (I_{to}) and the atrial-selective, ultrarapidly activating potassium current (I_{Kur}) (Burashnikov et al., 2004; Ravens and Wettwer, 2011). These currents dominate the early repolarization phase and lead to the typical spike and dome shape of the atrial AP. In notable contrast, hiPSC-aCM resulting from various RA-supplemented differentiation protocols exhibited a rather triangular AP shape without the prominent spike (Argenziano et al., 2018; Goldfracht et al., 2020; Gunawan et al., 2021; Honda et al., 2021; Pei et al., 2017), indicating incomplete atrial differentiation. In our own hands, the AP shape of engineered heart tissue (EHT) from hiPSC-aCM showed strong inter-investigator variability, indicating methodological issues during the differentiation process. Given the established key role of RA, we set out to prospectively investigate the concentration-dependent effects of RA on amplitudes of the atrial selective I_{Kur} in hiPSC-aCM. The contribution of I_{Kur} and $I_{K,ACh}$ to repolarization was estimated from AP recordings, which were measured in intact atrial-like EHT (aEHT).

RESULTS

To study the concentration dependency of RA on atrial specification, we added RA at 0.01, 0.1, or 1 μM after mesodermal induction of hiPSC for 3 days (Lemme et al., 2018). Cells cultured in the absence of RA were used as controls. We followed a standard embryoid body-based spinner protocol for cardiac differentiation of hiPSC (Breckwoldt et al., 2017). After EB dissociation, EHTs were casted and cultured for 4 weeks before they were used for either AP recordings or patch clamping in dissociated hiPSC-CM.

Concentration-dependent effects of RA on outward currents

In human hearts, outward currents are larger in atrial than in ventricular CMs, partially because of the expression of the atrial-selective I_{Kur} in atria (Amos et al., 1996). To quantify the effects of RA on atrial differentiation, we measured outward currents in hiPSC-CM differentiated in the presence of different concentrations of RA and in controls (differentiated in the absence of RA). We separated I_{Kur} from total outward current by applying a low concentration of the non-selective potassium channel blocker 4-AP (50 μM). Experiments were finished by 5 mM 4-AP to block not only I_{Kur} but also I_{to}.

We found I_{to}s in all individual hiPSC-CM (Figures 1A and 1B). In hiPSC-CM derived from an RA-free differentiation protocol, peak outward currents were not suppressed by 50 μM 4-AP, indicating an absence of I_{Kur}. Even the lowest concentration of RA (0.01 μM) was able to induce an outward current component sensitive to 50 μM 4-AP: I_{Kur} (3.5 ± 1.2; n = 16). Cells treated with higher RA concentrations showed progressively more I_{Kur} (with 1 μM RA, 12.1 ± 2.5 pA/pF; n = 16), but also I_{to} (difference between the current in the presence of 50 μM 4-AP and the current in the presence of 5 mM 4-AP, 33.5 ± 6.5 pA/pF; n = 16) and in a 4-AP-insensitive outward current component.

Large I_{to}s are needed to recapitulate the high repolarization fraction and low plateau voltage typical for human atrium

To investigate whether the RA-induced increase in outward currents is able to reproduce the typical spike and dome shape of the human atria, we measured AP by sharp microelectrodes in intact EHT casted from hiPSC-CM (ERC001) differentiated in the absence and in the presence of different concentrations of RA. EHTs from hiPSC-CM differentiated in the presence of RA beat faster without differences between RA groups (Figure 2B). Take-off potentials were less negative in EHT cultured with 0.1 and 1 μM RA than in those cultured with 0.01 μM or in the absence of RA (Figure 2). Effects of RA were more pronounced on APD. Even with a low RA concentration (0.01 and 0.1 μM), the APD_{90} was shorter than in the control group. Similar shortening of the APD at 20% repolarization (APD_{20}) and APD_{90} resulted in an unchanged repolarization fraction (APD_{90} – APD_{20}/APD_{90}) in these two groups (Figure 2). In contrast, EHT casted from hiPSC-CM differentiated in the presence of 1 μM RA had a drastically shorter APD_{20} without further shortening of the APD_{90}, leading to the typical spike and dome AP shape of adult human atrium and a lower repolarization fraction (Figure 2). Thus, a critical concentration of RA (1 μM) is necessary and sufficient to induce a typical human atria-like AP shape in hiPSC-aCM in the EHT format. The steep concentration dependency of the RA effect was confirmed in another cell line (ERC021) (Figure S2; Tables S1–S3).

Large I_{to}s are required to recapitulate I_{Kur} block response pattern as seen in human atrium

In human atrium, blocking the I_{Kur} shifts the plateau voltage to less negative values and leads to a seemingly paradoxical abbreviation of terminal repolarization, i.e., a decrease in APD_{90}, because another important potassium current (I_{Kr}) becomes more strongly activated at the less negative plateau voltage (Wettwer et al., 2004). To assess how much RA is needed to reproduce this pattern, we measured the effects of I_{Kur} block (50 μM 4-AP) in EHT casted from hiPSC-CM (ERC001) differentiated in the absence or presence of RA (0.01, 0.1, and 1 μM). In controls (0 RA), 50 μM 4-AP did not change APD (APD_{20} or APD_{90}) or plateau voltage (Figure 3). In contrast, 4-AP prolonged APD_{20} in all three RA groups, indicating that even low concentrations of RA induce a relevant contribution of the atrial-selective I_{Kur} to repolarization. Only in EHT casted from hiPSC-CM differentiated in the presence of 1 μM RA, blocking of I_{Kur} shifted the plateau voltage to less negative values accompanied by shortening in APD_{90}, i.e., the canonical pattern of adult human atrium. These results were confirmed in another cell line (ERC021) (Figure S3; Table S2).

To investigate whether the shortening of APD_{90} upon I_{Kur} block in EHT (1 μM RA) is mediated by I_{Kr}, we repeated experiments in the presence of the I_{Kr} blocker E-4031 (1 μM). I_{Kr} block alone prolonged APD_{90}, but not APD_{20}. E-4031 did not affect the plateau voltage. As seen before in the absence of E-4031, I_{Kur} block by 50 μM 4-AP shifted the plateau voltage to less negative values when given on top of E-4031. However, under this condition, 4-AP no longer a shortened, but a prolonged, APD_{90} (Figure 4).

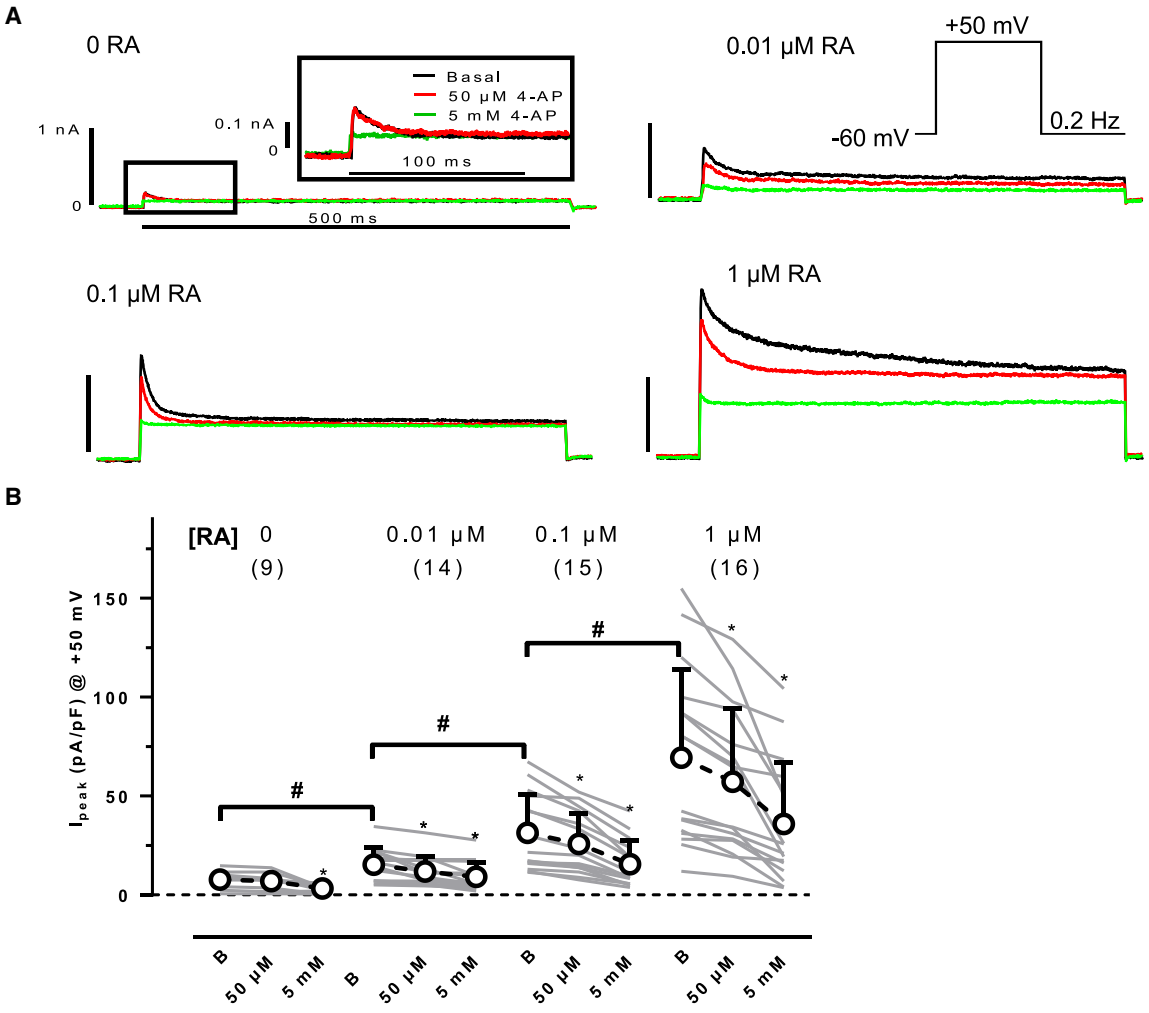

Figure 1. Concentration dependency of RA on outward currents in hiPSC-CM

(A) Original current traces recorded in individual hiPSC-CM differentiated in the absence (0 RA) or presence of different concentration of RA in in the absence (basal) and in the presence of 50 µM 4-AP and 5 mM 4-AP. For 0 RA, the initial part of outward currents is given on an extended scale. Pulse protocol given as inset.

(B) Summary of the results for peak currents measured in the absence of 4-AP (basal) (B) and in the presence of 50 µM and 5 mM 4-AP, recorded in hiPSC-CM cultured with different concentrations of RA (concentration given on top). Gray lines indicate individual cells (number of cells given in brackets, dissociated from three EHTs, generated from three different batches). Open circles indicate mean values ± SD. *$p < 0.05$ (repeated measures ANOVA) vs respective basal values. #$p < 0.05$ (one-way ANOVA of log-transformed data).

Low concentrations of RA are insufficient to produce relevant APD shortening upon muscarinic receptor activation

Besides I_{Kur}, the physiology of human atria is characterized by the expression of large acetylcholine-sensitive inward rectifying ion currents, I_{KACh}. To assess $I_{K,ACh}$ contribution to the AP shape, we measured AP responses to 10 µM carbachol (CCh) in EHT (ERC001) from the three RA groups. We found a slight, but significant, decrease in the beating rate upon CCh in all three groups (Figure 5). However, only in EHT of the 1 µM RA group, CCh significantly decreased APD_{90} and shifted take-off potential (TOP) to more negative values (Figure 5). The results were confirmed in another cell line (ERC021) (Figure S4; Table S3).

To investigate whether 1 µM RA has a uniform effect on the occurrence of $I_{K,ACh}$ in hiPSC-CM (ERC001) differentiated with RA, we measured CCh responses of inward rectifier currents in single hiPSC-aCM (isolated from EHT of the 1 µM RA group only). The current density, measured at −100 mV, before adding CCh was 7.7 ± 0.9 pA/pF (n = 34). We saw a rapid increase in inward rectifier current upon exposure to CCh (Figure 6). There was a large scatter in effect size between individual cells,

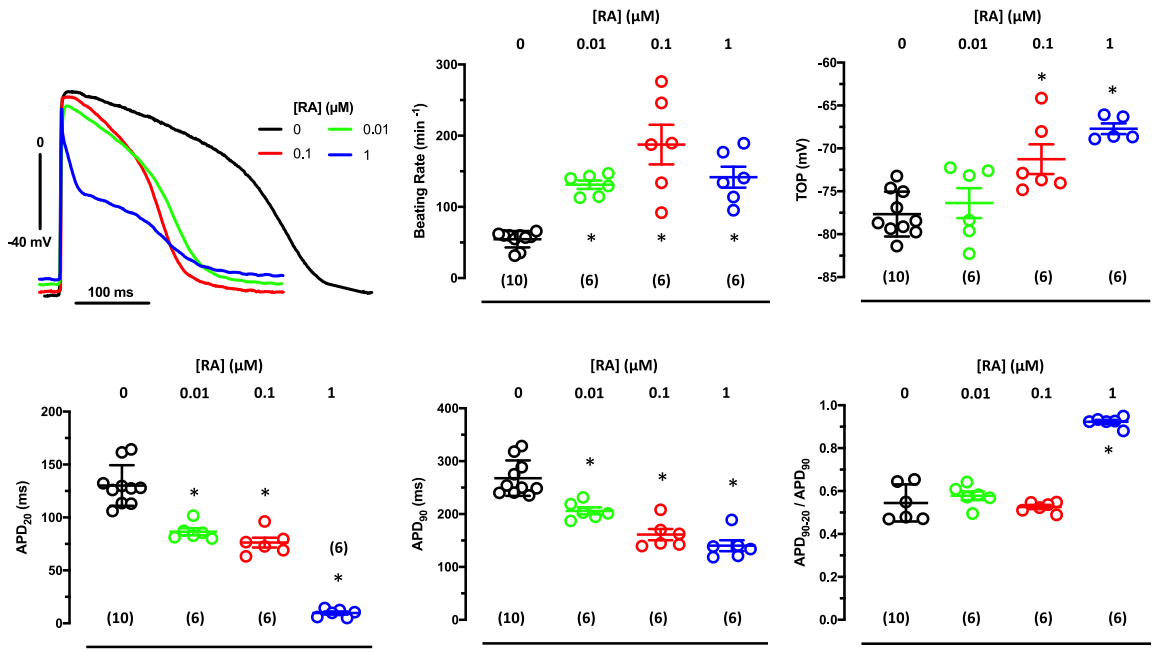

Figure 2. Concentration dependency of RA on AP in EHT

(Top) Superimposed original traces of AP recorded in EHT (ERC001) based on hiPSC-CMs cultured in the absence (0) or presence of RA concentrations. Summary of results: Mean values ± SD for beating rate (BR). (Bottom) AP duration (APD_{20} and APD_{90}) and repolarization fraction (APD_{90} – APD_{50}/APD_{90}). *p < 0.05 vs 0 RA (one-way ANOVA of log-transformed data). Number of EHTs resulting from one differentiation run is given in brackets. Individual data points represent single AP recording from one individual EHT.

but all cells showed an increase. The mean current density more than doubled (to 18.9 ± 2.1 pA/pF; $p < 0.05$, paired t-test), indicating robust and uniform expression of $I_{K,Ach}$ in hiPSC-CM when differentiated in the presence of 1 µM RA.

Loss of RA by sterile filtration

Given the obvious discrepancies between the present results and our own study using a very similar methodology (Lemme et al., 2018), we carefully compared experimental procedures and identified sterile filtration of stock solution of RA in the prior study to be the only apparent difference. We suspected sterile filtration may lead to a substantial loss of RA concentration in stock solutions. We, therefore, measured the effect of sterile filtration on RA concentration by three different filters. All three filters adsorbed a significant amount of RA (Table S4). When using a PETF filter, RA recovery was only about 0.1%.

Reproducibility of RA effects on AP shape

We have addressed the issue of reproducibility of RA-treatment on AP shape in a larger number of EHT generated from three different batches (both RA treated and non-treated) from three different cell lines (ERC001, ERC018, and ERC021). RA treatment at 1 µM induced an atrial-like AP shape (plateau voltage [$V_{Plateau}$] < 0 mV, APD_{20} < 15 ms, and repolarization fraction close to 1) in all three batches of three cell lines (Figure 7). There was no overlap in the selected parameters between EHT from hiPSC-CM treated with or without RA.

DISCUSSION

Our study has three major conclusions.

1. A concentration of 1 µM RA is sufficient and necessary to induce a fully human-like atrial AP phenotype in hiPSC-CM under our experimental conditions, i.e., low growth factor combination in the atrial CM differentiation protocol and EHT (3D).
2. Sterile filtration of RA can lead to a relevant loss of RA preventing induction of the adult atrial AP phenotype.
3. Sharp microelectrode measurements in intact tissues (EHT) are critical to reproduce the canonical interplay between I_{Kur} and I_{Kr} as known from human atria.

RA is crucial to induce atrial differentiation in hiPSC-CM, and several groups have used the shape of AP as proof of an atrial phenotype in RA-treated hiPSC-CM (Table S5). While it is clear that all studies show RA-induced effects on AP parameters toward a human atrial phenotype when compared with CM from standard differentiation

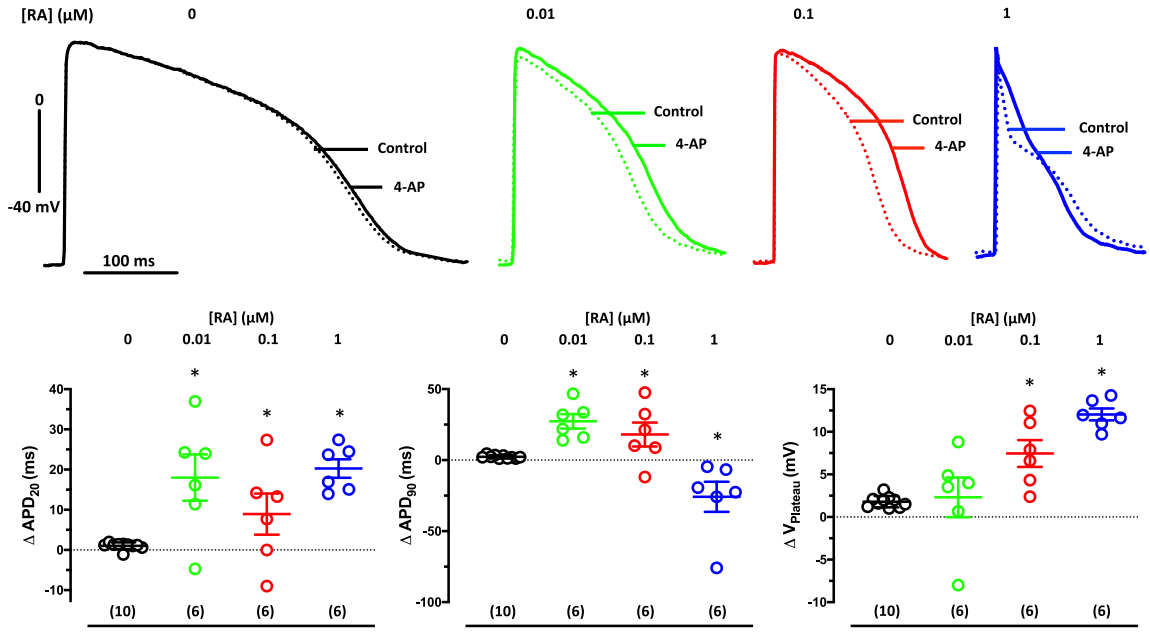

Figure 3. Concentration dependency of RA on the AP response to I_{Kur} block

(Top) Superimposed original traces of AP before (control) and after exposure to 50 µM 4-AP in EHT based on hiPSC-CM (ERC001) cultured in the absence (0 RA) or in the presence of RA (concentration given in brackets). (Bottom) Summary of results for the effects of 4-AP on APD_{20} (left), on $V_{Plateau}$ (middle), and on $APD_{90;}$ (right). Open circles indicate mean values ± SD. Numbers in brackets indicate number of EHTs resulting from one differentiation run. *p < 0.05 vs 0 RA (one-way ANOVA of log-transformed data). Individual data points represent single AP recording from one individual EHT.

protocols, the atrial myocyte likeness varies widely. We discuss some points that could be relevant for the inconsistencies.

Effects of cell source (hESC vs hiPSC) and culture conditions (3D vs 2D)

It seems reasonable to suspect an impact of cell source on the success of RA to induce an atrial AP phenotype. Three of seven papers that reported in detail the effects of RA on AP shape have used hESC (Devalla et al., 2015; Laksman et al., 2017; Zhang et al., 2011); the other four studies used hiPSC (Cyganek et al., 2018; Goldfracht et al., 2020; Lee et al., 2017; Lemme et al., 2018). Data on the APD_{20} are available from most studies (Table S5). The APD_{20} was consistently short in both studies based on hESC (Devalla et al., 2015; Laksman et al., 2017), but varied widely when hiPSC were used. The data could indicate that RA effects are less robust in hiPSC, but the current data in hiPSC argue against this idea. Alternatively, the biology of individual hiPSC lines may vary more than that of hESC lines.

Direct head-to-head comparisons of 2D and 3D culture conditions are, to the best of our knowledge, limited to an earlier study by our group, but here the effects of RA were more pronounced in 3D EHTs than 2D monolayers, both in terms of atrial gene expression patterns and repolarization fraction (Lemme et al., 2018). In contrast, three of the four studies on RA-treated hESC-CM/hiPSC-CM cultured in 2D format reported APD_{20} values between 13 and 37 ms, close to the situation in human atrium (Devalla et al., 2015; Laksman et al., 2017; Lee et al., 2017), indicating that RA is able to induce a strong, atrial-like early repolarization in the 2D format as well.

Recording techniques and other methodological conditions

We measured AP in intact EHT with sharp microelectrodes, while AP in hESC-aCM and hiPSC-aCM were mostly assessed by patch clamp recordings in isolated cells. This methodological difference may be critical. We observed previously that data scatter of the APD and resting membrane potential was much greater when APs were measured in isolated cells compared with intact tissues (Horváth et al., 2018). The parameter repolarization fraction loses its power to discriminate between adult human ventricle and atrium when APs were measured in individual cells (Horváth et al., 2018).

Enzymatic isolation of cells may be an important reason for the observed differences between single cells and intact tissues. Devalla et al. (2015) reported a short APD_{20} and a strong effect of 4-AP at 50 µM (including an upward shift

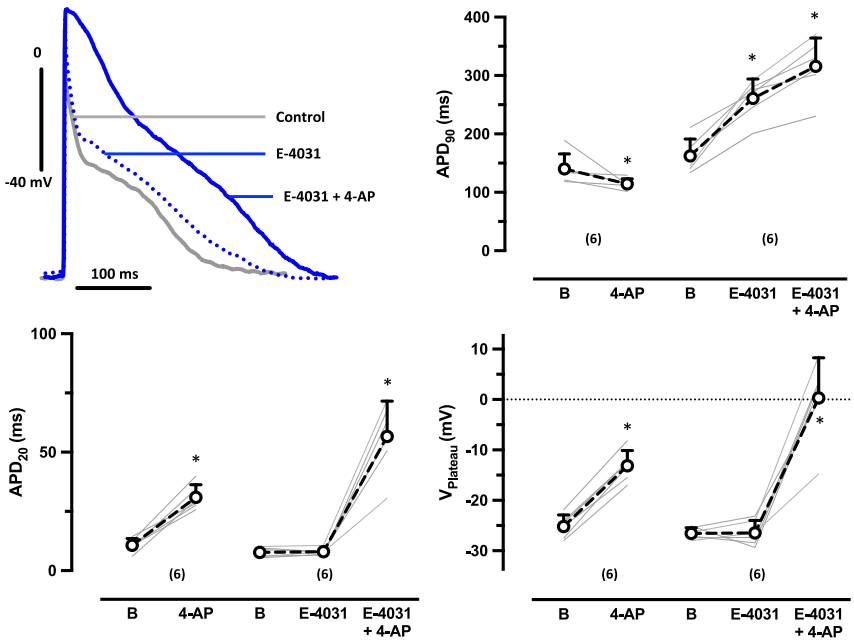

Figure 4. In aEHT (1 μM RA)m the I_{Kur} block-induced shortening of APD_{90} depends on I_{Kr}

(Top left) Superimposed original traces of AP in EHT based on hiPSC-CM (ERC001) treated with 1 μM RA before (basal) (B) and after exposure to 50 μM 4-AP in the presence of the I_{Kr} blocker E-4031 (1 μM) (right). Summary of results for the effects of 4-AP in the absence and presence of E-4031 on APD_{90} (top left), on APD_{20} (bottom left), and on $V_{Plateau}$ (bottom right). Gray lines indicate individual EHT. Numbers in brackets indicate number of EHTs resulting from one differentiation run. Open circles indicate mean values ± SD. *p < 0.05 vs basal or E-4031, respectively (paired t-test).

of $V_{Plateau}$, like in this study and in the human adult atrium), but the APD_{90} was prolonged in the presence of 4-AP instead of the expected shortening. This finding strikingly resembles the situation we report here obtained in the presence of E-4031. The I_{Kur} block-induced shortening of APD_{90} depends on I_{Kr}, both in the human adult atrium

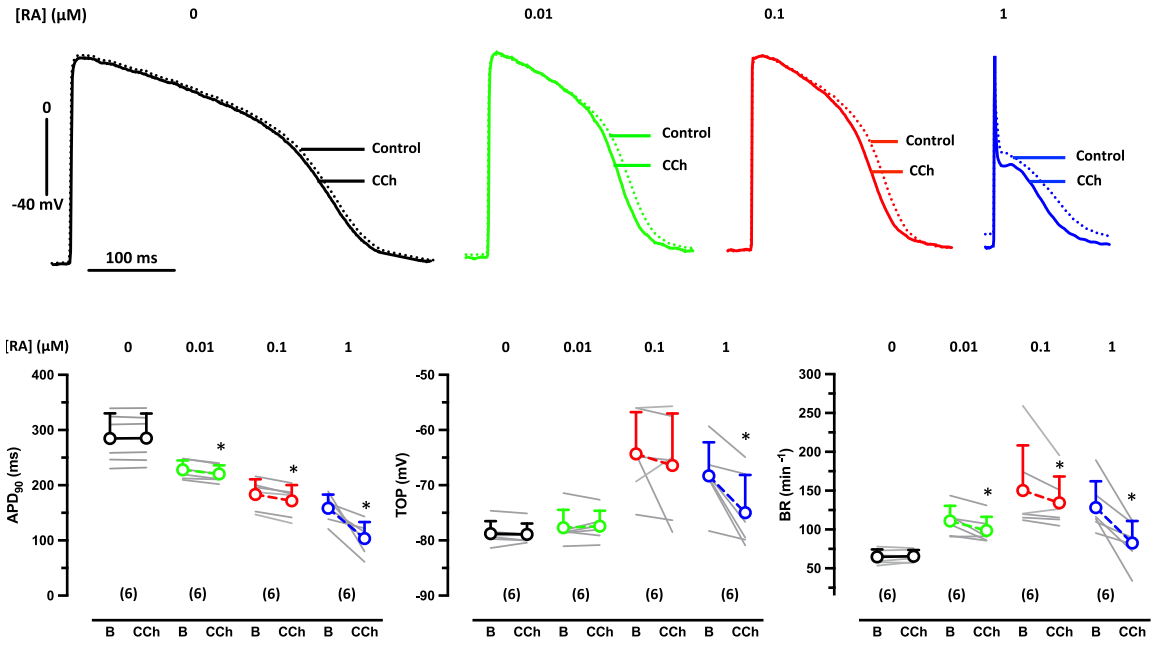

Figure 5. Concentration dependency of RA on CCh effects on APD_{90} in EHT

(Top) Superimposed original traces of AP before (basal) (B) and after exposure to 10 μM CCh recorded in EHT based on hiPSC-CM (ERC001) cultured in the presence of 0.01, 0.1, and 1 μM RA. (Bottom) Summary of results for the effects of CCh on beating rate (BR) (left), TOP (middle), and APD_{90} (right). Gray lines indicate individual EHT. Numbers in brackets indicate number of EHTs resulting from one differentiation run. Open circles indicate mean values ± SD. *p < 0.05 vs basal (paired t-test). Number of EHTs is given in brackets. Individual data point represents single AP recording from one individual EHT.

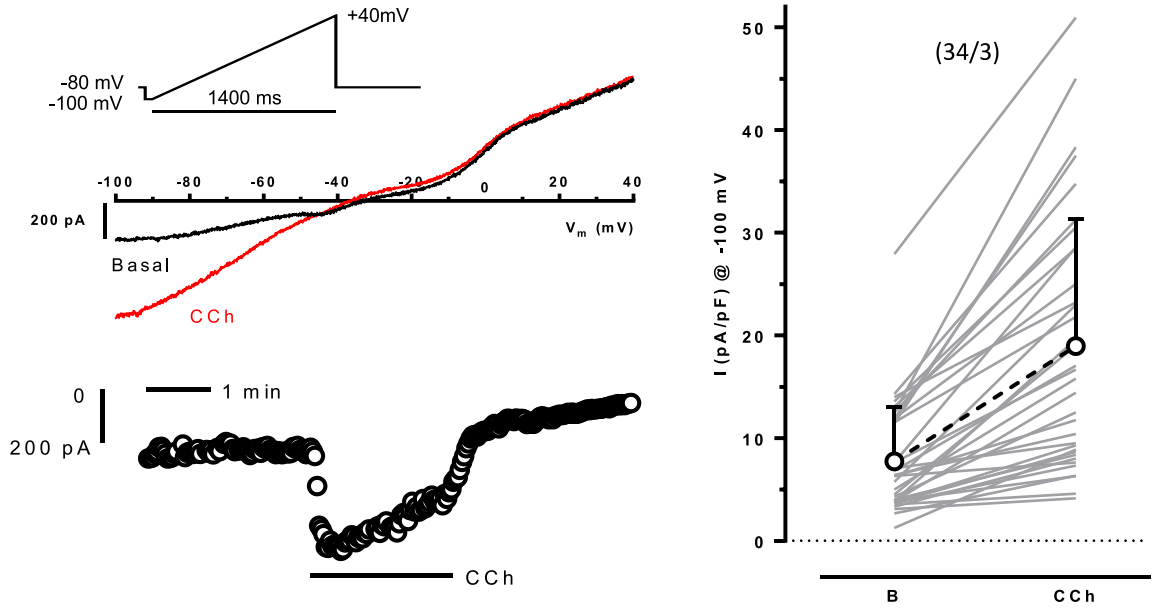

Figure 6. Consistent increase of inward rectifier currents upon CCh in hiPSC-CM (1 μM RA)

(Top left) Superimposed original current traces evoked by a slow voltage ramp in a hiPSC-CM cultured (ERC001) in the presence of 1 μM RA before (basal) and after exposure to 10 μM CCh. Pulse protocol given as inset. (Bottom left) Time course of the current at −100 mV in response to CCh. (Right) Summary of results for the current at −100 mV. Gray lines indicate individual hiPSC-aCM, open circles indicate respective mean values ± SD. Numbers in brackets indicate number of cells/number of dissociated EHTs (three different batches). *$p < 0.05$ vs basal (paired t-test).

(Wettwer et al., 2004) and in hiPSC-aCM (Figure 4). Importantly, the hERG channel that mediates I_{Kr} can be easily destroyed by enzymes frequently used for cell isolation. In fact, I_{Kr} currents disappeared within minutes when cells were superfused with protease XIV, protease XXIV, proteinase K, or trypsin (Rajamani et al., 2006). Devalla et al (2015) used a commercial kit (TrypLE Select Enzym, catalog no. 12563011, ThermoFisher) that contains a not further defined protease.

Different effects of I_{Kur} block: Measurements in intact tissues as gold standard

The blocking of I_{Kur} results in different effects upon the respective methodological conditions: in intact atrial tissues, both human right atrial appendages (Wettwer et al., 2004; Christ et al., 2008; Ford et al., 2013; Loose et al., 2014; Ford et al., 2016) and atrial EHT (Schulz et al., 2023; and this study), the blocking of I_{Kur} resulted in APD_{90} shortening when sharp microelectrodes were used for the AP recordings. In contrast, APs recorded by patch clamp in both isolated human adult atrial CMs (Lagrutta et al., 2006; Verkerk et al., 2021) and isolated atrial hiPSC-CMs (Hilderink et al., 2020) were prolonged upon I_{Kur} blocking. The enzymatic dissociation could be a possible explanation for the observed difference. Therefore, it seems justified to speculate that enzymatic dissociation of both adult human atrial CMs and atrial hiPSC-CMs may have abolished the I_{Kr}-mediated APD_{90} shortening and changed the response pattern to I_{Kur} block. Furthermore, the respective recording technique (patch clamp vs sharp microelectrode) could be another explanation for the APD_{90} prolongation instead of shortening upon I_{Kur} block. Since AP measurements by sharp microelectrodes in intact tissues remain the gold standard and are still important in safety pharmacology, we favor this recording technique for the validation of a full atrial electrophysiological phenotype induced by RA during atrial hiPSC-CM differentiation.

Loss of RA by sterile filtration

We saw a substantial loss of RA by sterile filtration. The effects are so large that we would no longer expect full effects of RA on differentiation. We do not know whether loss of RA by sterile filtration contributed to the variability between different studies, because no information is provided in the respective papers, but we consider it a possibility. In our own previous study, we felt safe to filter the RA solution because the manufacturers states in its official product information that "Mahady and Beecher report sterile filtering RA solutions before addition to suspension cells" (Sigma, 1996). However, RA recovery after sterile filtration was not reported in the cited paper

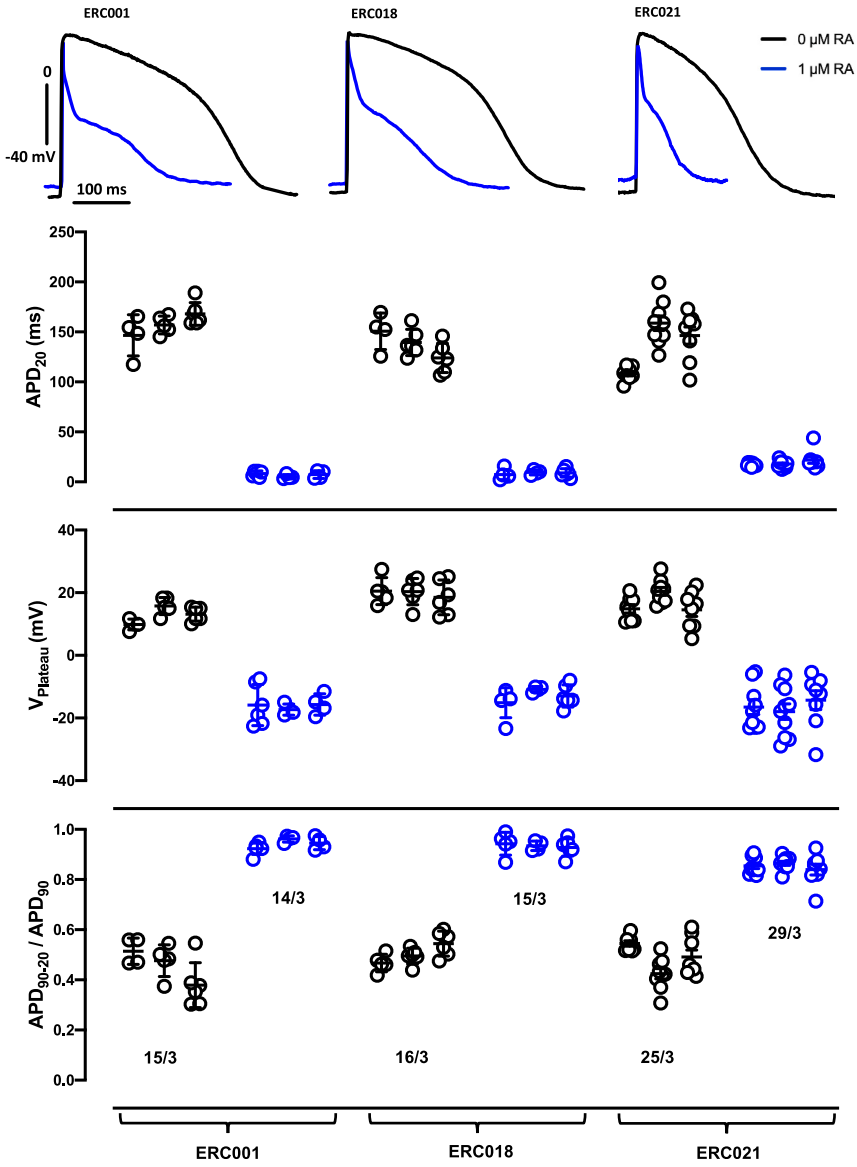

Figure 7. Reproducibility of RA-effects on AP shape

(Top) Original recordings of AP recorded in EHT based on hiPSC-CM differentiated with 0 and 1 µM RA from three different cell lines (ERC001, ERC018, and ERC021).

(Bottom) Individual data points and mean values ± SD for AP duration at APD_{20}, $V_{Plateau}$, and repolarization fraction (APD_{90} – APD_{20}/APD_{90}) measured in EHT from three different batches of RA-treated (1 µM RA) vs untreated hiPSC-CM (0 RA) from three different cell lines. Individual data point represents single AP recording from one individual EHT. *$p < 0.05$ for nested ANOVA vs 0 RA of the same cell line. #No significant difference between single batches (ANOVA, every batch against another). n/N indicate number of EHTs/number of different batches.

(Mahady and Beecher, 1996). Also, no details on the filter material were given in that study. At least contemporarily used sterile filters absorb large amounts of RA. Thus, it seems wise to determine RA recovery or to refrain from sterile filtration of RA-containing solutions.

Limitations of the study

We cannot exclude the possibility that changes in currents other than I_{Kur} or $I_{K,ACh}$, e.g., other outward currents, may have contributed to the effects of RA on repolarization. We did not measure the effects of RA treatment on gene expression. We were not able to measure APD at 1 Hz; even under ivabradine, we could not slow down substantially the spontaneously beating rate in all three RA-treated cell lines. Loss of rate adaptation of APD is a key finding in persistent AF. More important, the APD_{90} in human persistent AF is only shorter when measured at low rates (approximately 1 Hz). Thus, the inability to record APD at 1 Hz in hiPSC-aCM is a substantial limitation when this model is used to characterize remodeling (Lemoine et al., 2018).

EXPERIMENTAL PROCEDURES

Resource availability

Corresponding author

Further information and requests for resources and reagents should be directed to and will be fulfilled by the corresponding author, Thomas Eschenhagen (t.eschenhagen@uke.de).

Materials availability

This study did not generate new unique reagents. All stable reagents generated in this study are available from the lead contact with a completed Materials Transfer Agreement.

Data and code availability

No standardized datasets or codes were generated in this study.

Atrial differentiation of hiPSC and generation of atrial EHT

For all experiments, three healthy in house control cell lines (ERC001, ERC018, and ERC021) were used (EBiSC: UKEi001-A [https://hpscreg.eu/cell-line/UKEi001-A], EBiSC: UKEi018-A [https://hpscreg.eu/cell-line/UKEi018-A], and UKEi021-A [https://hpscreg.eu/cell-line/UKEi021-A]). All experimental methods for these procedures were approved by the Ethical Committee of the University Medical Center Hamburg-Eppendorf (Az. PV4798, 28.10.2014). All patients gave written informed consent. Protocols for hiPSC expansion, atrial CM differentiation, and EHT generation for both hiPSC lines were performed as previously described (Breckwoldt et al., 2017). IPS cell lines were derived from dermal fibroblasts from healthy probands. In brief, embryoid bodies (EBs) were generated from expanded hiPSCs using spinner flasks and stirred suspension. Mesodermal induction was performed by a growth factor cocktail. While the basic fibroblast growth factor concentration was the same in all groups (5 ng/mL), BMP-4 and activin A concentrations were slightly lower in the RA-based atrial differentiation protocol when compared with our standard ventricular differentiation protocol without RA (Breckwoldt et al., 2017) (2 instead of 3 ng/mL BMP-4 and 5 instead of 10 ng/mL activin A, respectively). Growth factors were given for 3 days. For the induction of atrial CM differentiation, RA (0.01, 0.1, or 1 μM) was added for the first 72 h of WNT signaling inhibition, as recently described (Lemme et al., 2018). RA (Sigma Aldrich R2625) was dissolved in DMSO (stock concentration 100 μM) and used without sterile filtration. The differentiation run for all hiPSC treated with different RA-concentrations and for the respective control (0 RA) were prospectively performed in parallel. In one cell line (ERC021), we tried 10 μM RA during mesodermal induction, but those hiPSC-CM did not start beating.

After successful differentiation, dissociation of EBs was performed with collagenase II (200 U/L, Worthington, LS004176 in Hank's balanced salt solution minus Ca^{2+}/Mg_{2+}, Gibco, 14175-053 3.5 h, normoxia, 37°C) (Breckwoldt et al., 2017). EBs were incubated with collagenase for 3.5 h (37°C, normoxia) and were dispersed to isolated atrial CMs (hiPSC-aCM).

aEHT was generated from 1 million hiPSC-aCMs per construct. The fibrin gel matrix was made by mixing hiPSC-aCM, fibrinogen (Sigma F4753) and thrombin (100 U/L, Sigma Aldrich T7513), which were poured into agarose (1%) casting molds with silicone posts inserted from above (Breckwoldt et al., 2017; Hansen et al., 2010; Lemme et al., 2018).

AP measurement

AP measurements were performed with standard sharp microelectrodes as described previously (Lemoine et al., 2018; Wettwer et al., 2013). All measurements were done in aEHTs, which were continuously superfused with Tyrode's solution (NaCl 127 mM, KCl 5.4 mM, $MgCl_2$ 1.05 mM, $CaCl_2$ 1.8 mM, glucose 10 mM, $NaHCO_3$ 22 mM, $NaHPO_4$ 0.42 mM, and balanced with O_2-CO_2 [95:5] at 36°C, pH 7.4). The sharp microelectrode consisted of filamented borosilicate glass capillaries with an external diameter of 1.5 mm and internal diameter of 0.87 mm (HILG1103227; Hilgenberg). The DPZ-Universal puller (Zeitz Instruments) was used to fabricate microelectrodes that had a resistance between 25 and 55 MΩ when filled with 2 M KCl. The pipettes were controlled by a hydraulic micromanipulator (Narishige MO-203), ensuring a delicate contact with the tissue. The aEHTs were transferred from the 24-well EHT culture plate into the AP measuring chamber by cutting the silicone posts and were fixed with needles in an optimal position for AP recording. The signals were amplified by a BA-1s npi amplifier (npi electronic GmbH). APs were recorded and analyzed using the Lab-Chart software (version 5, AD Instruments Pty Ltd.). Definition of $V_{Plateau}$ (Ford et al., 2013) was slightly modified as the voltage at in the range of ±5 ms time at approximately 30% of the APD_{90}. The TOP was defined as the diastolic membrane potential directly before the upstroke.

Current measurements

Ion currents were measured at 37°C using the whole-cell configuration of the patch-clamp technique by an Axopatch 200B amplifier (Axon Instruments). The ISO2 software was used for data acquisition and analysis (MFK). Heat-polished pipettes were pulled from borosilicate filamented glass (Hilgenberg). Tip resistances were 2.5–5 MΩ, seal resistances were 3–6 GΩ. Cell capacitance was calculated from steady-state current during depolarizing ramp pulses (1 V/1 s) from −40 to −35 mV. Human iPSC-CMs used for patch clamp measurements were dissociated from EHTs by collagenase II (200 U/mL; Worthington Biochemical) for 5 h at 37°C, 21% oxygen, and 5% CO_2. Isolated cells were plated on gelatine-coated (0.1%) glass coverslips (12 mm diameter; Carl Roth GmbH + Co) and kept in culture for 24–48 h to maintain adherence under superfusion in the recording chamber during patch clamp measurements. The cells were investigated in a small perfusion chamber placed on the stage of an inverse microscope. Inward rectifier currents were measured with the following bath solution: NaCl 120 mM, KCl 20 mM, HEPES 10 mM, $CaCl_2$ 2 mM, $MgCl_2$ 1 mM, and glucose 10 mM (pH 7.4, adjusted with NaOH). Contaminating Ca^{2+} currents were suppressed with the selective L-type calcium channel blocker nifedipine (10 μM). The internal solution included DL-aspartate potassium salt 80 mM, KCl 40 mM, NaCl 8 mM, HEPES 10 mM, Mg-ATP 5 mM, Tris-GTP 0. mM 1, EGTA 5 mM, and $CaCl_2$ 2 mM, pH 7.4, adjusted with KOH. Inward current amplitudes were determined as currents at −100 mV (Horváth et al., 2018). A single concentration (2 μM) of the muscarinic receptor agonist CCh was used to evoke $I_{K,ACh}$. I_{to}s were measured in a slightly modified bath solution (KCl 5.4 mM instead of 20 mM). Currents were elicited by 500-ms-long test pulses to +50 mV applied every 5 s from a holding potential of −60 mV (Christ et al., 2008). Cells were exposed to two concentrations of 4-AP (50 μM and 5 mM).

Sterile filtration and mass spectrometry

We prepared RA stock solutions (100 μM) in DMSO. One milliliter of this solution was filtered through three different sterile filters: Filtropur S (pore size 0.2 μm, polyethersulfon; Saarstedt), Millex-GP (pore size 0.22 μM, polyethersulfon; Merck Millipore Ltd.)m and Whatman REZIST (pore size 0.2 μm, polytetrafluorethen; Cytiva). An unfiltrated solution was used as control.

RA was quantified by liquid chromatography-tandem mass spectrometry (LC-MS/MS) as described previously (Morgenstern et al., 2021). Stock solutions of RA and internal standard, i.e., all-trans RA-d5 (Cayman Chemical), were made up in DMSO (1 mg/mL). Calibration curves ranged from 10 to 1,000 ng/mL, five levels. We added 20 μL calibrator or sample to 1.5-mL Eppendorf tubes and 20 μL all-trans RA-d5 at 1,000 ng/mL were added to each tube and vortexed briefly. We added 200 μL acetonitrile to each tube and vortexed for 1 min prior to centrifugation for 10 min at 13,000 rpm. We transferred 100 μL supernatant to an MS 96-well plate with 20 μL water and capped it. LC was performed applying a gradient of 0.8 mL/min 25/75%, v/v %, A (0.1% formic acid) and B (acetonitrile/methanol, 50/50), to 2/98% over 2:50 min:sec on a Luna 5-μm C18 50 × 2.0-mm 100 A column (Phenomenex). For MS/MS analyses in the positive electrospray ionization mode on a Varian 1200 TSQ (Agilent Technologies), the transitions m/z 301.2 > 123.0 @18 eV and m/z 306.2 > 127.0 @18 eV were monitored for RA and internal standard; concentrations were calculated by peak area ratio determination of calibrators and samples.

Statistics

Statistical analyses were performed by using GraphPad Prism software version 7 (GraphPad Software). Data are presented as mean ± SD. Log transformation was used to allow application of parametric testing of data (Ismaili et al., 2020). Statistical significance was considered for differences with a p value of less than 0.05.

SUPPLEMENTAL INFORMATION

Supplemental information can be found online at https://doi.org/10.1016/j.stemcr.2023.10.006.

ACKNOWLEDGMENTS

The authors thank Anna Steenpaß for excellent help with patch-clamp measurements and technical support in action potential recordings. We are grateful to Birgit Klampe and Thomas Schulze for help with CM differentiation. This work was supported by a grant provided by the German Centre for Cardio- vascular Research (grant No. 81Z0710110 to C. Schulz) and by the European Research Council (ERC-AG IndivuHeart).

AUTHOR CONTRIBUTIONS

C.S., J.K., B.P., A.H., T.E., D.A., and T.C. planned experiments; C.S., M.S. T.E., D.A., and T.C. contributed to experiments and data analysis. C.S., T.E., and T.C. wrote the manuscript. All authors approved the final version of the manuscript.

DECLARATION OF INTERESTS

T.E. is consultant and shareholder of Dinaqor AG.

Received: July 27, 2022
Revised: October 5, 2023
Accepted: October 9, 2023
Published: November 2, 2023; corrected online: November 14, 2023

REFERENCES

Amos, G.J., Wettwer, E., Metzger, F., Li, Q., Himmel, H.M., and Ravens, U. (1996). Differences between outward currents of human atrial and subepicardial ventricular myocytes. J. Physiol. *491*, 31–50. Pt 1. https://doi.org/10.1113/jphysiol.1996.sp021194.

Argenziano, M., Lambers, E., Hong, L., Sridhar, A., Zhang, M., Chalazan, B., Menon, A., Savio-Galimberti, E., Wu, J.C., Rehman, J., and Darbar, D. (2018). Electrophysiologic Characterization of Calcium Handling in Human Induced Pluripotent Stem Cell-Derived Atrial Cardiomyocytes. Stem Cell Rep. *10*, 1867–1878. https://doi.org/10.1016/j.stemcr.2018.04.005.

Breckwoldt, K., Letuffe-Brenière, D., Mannhardt, I., Schulze, T., Ulmer, B., Werner, T., Benzin, A., Klampe, B., Reinsch, M.C., Laufer, S., et al. (2017). Differentiation of cardiomyocytes and generation of human engineered heart tissue. Nat. Protoc. *12*, 1177–1197. https://doi.org/10.1038/nprot.2017.033.

Burashnikov, A., Mannava, S., and Antzelevitch, C. (2004). Transmembrane action potential heterogeneity in the canine isolated arterially perfused right atrium: Effect of IKr and I Kur/Ito block. Am. J. Physiol. Heart Circ. Physiol. *286*, 2393–2400. https://doi.org/10.1152/ajpheart.01242.2003.

Christ, T., Wettwer, E., Voigt, N., Hála, O., Radicke, S., Matschke, K., Várro, A., Dobrev, D., and Ravens, U. (2008). Pathology-specific effects of the IKur/Ito/IK,ACh blocker AVE0118 on ion channels in human chronic atrial fibrillation. Br. J. Pharmacol. *154*, 1619–1630. https://doi.org/10.1038/bjp.2008.209.

Cyganek, L., Tiburcy, M., Sekeres, K., Gerstenberg, K., Bohnenberger, H., Lenz, C., Henze, S., Stauske, M., Salinas, G., Zimmermann, W.H., et al. (2018). Deep phenotyping of human induced pluripotent stem cell-derived atrial and ventricular cardiomyocytes. JCI Insight *3*, e99941. https://doi.org/10.1172/jci.insight.99941.

Devalla, H.D., Schwach, V., Ford, J.W., Milnes, J.T., El-Haou, S., Jackson, C., Gkatzis, K., Elliott, D.A., Chuva de Sousa Lopes, S.M., Mummery, C.L., et al. (2015). Atrial-like cardiomyocytes from human pluripotent stem cells are a robust preclinical model for assessing atrial-selective pharmacology. EMBO Mol. Med. *7*, 394–410. https://doi.org/10.15252/emmm.201404757.

Ford, J., Milnes, J., Wettwer, E., Christ, T., Rogers, M., Sutton, K., Madge, D., Virag, L., Jost, N., Horvath, Z., et al. (2013). Human electrophysiological and pharmacological properties of XEN-D0101: A novel atrial-selective Kv1.5/IKur inhibitor. J. Cardiovasc. Pharmacol. *61*, 408–415. https://doi.org/10.1097/FJC.0b013e31828780eb.

Ford, J., Milnes, J., El Haou, S., Wettwer, E., Loose, S., Matschke, K., Tyl, B., Round, P., and Ravens, U. (2016). The positive frequency-dependent electrophysiological effects of the IKur inhibitor XEN-D0103 are desirable for the treatment of atrial fibrillation. Heart Rhythm *13*, 555–564. https://doi.org/10.1016/j.hrthm.2015.10.003.

Goldfracht, I., Protze, S., Shiti, A., Setter, N., Gruber, A., Shaheen, N., Nartiss, Y., Keller, G., and Gepstein, L. (2020). Generating ring-shaped engineered heart tissues from ventricular and atrial human pluripotent stem cell-derived cardiomyocytes. Nat. Commun. *11*, 75. https://doi.org/10.1038/s41467-019-13868-x.

Gunawan, M.G., Sangha, S.S., Shafaattalab, S., Lin, E., Heims-Waldron, D.A., Bezzerides, V.J., Laksman, Z., and Tibbits, G.F. (2021). Drug screening platform using human induced pluripotent stem cell-derived atrial cardiomyocytes and optical mapping. Stem Cells Transl. Med. *10*, 68–82. https://doi.org/10.1002/sctm.19-0440.

Hansen, A., Eder, A., Bonstrup, M., Flato, M., Mewe, M., Schaaf, S., Aksehirlioglu, B., Schworer, A., Uebeler, J., Eschenhagen, T., et al. (2010). Development of a Drug Screening Platform Based on Engineered Heart Tissue. Circ. Res. https://doi.org/10.1161/CIRCRESAHA.109.211458.

Heidbüchel, H., Vereecke, J., and Carmeliet, E. (1987). The electrophysiological effects of acetylcholine in single human atrial cells. J. Mol. Cell. Cardiol. *19*, 1207–1219. https://doi.org/10.1016/S0022-2828(87)80531-X.

Hilderink, S., Devalla, H.D., Bosch, L., Wilders, R., and Verkerk, A.O. (2020). Ultrarapid Delayed Rectifier K+ Channelopathies in Human Induced Pluripotent Stem Cell-Derived Cardiomyocytes. Front. Cell Dev. Biol. *8*, 536. https://doi.org/10.3389/fcell.2020.00536.

Honda, Y., Li, J., Hino, A., Tsujimoto, S., and Lee, J.K. (2021). High-Throughput Drug Screening System Based on Human Induced Pluripotent Stem Cell-Derived Atrial Myocytes ~ A Novel Platform to Detect Cardiac Toxicity for Atrial Arrhythmias. Front. Pharmacol. *12*, 680618. https://doi.org/10.3389/fphar.2021.680618.

Horváth, A., Lemoine, M.D., Löser, A., Mannhardt, I., Flenner, F., Uzun, A.U., Neuber, C., Breckwoldt, K., Hansen, A., Girdauskas, E., et al. (2018). Low Resting Membrane Potential and Low Inward Rectifier Potassium Currents Are Not Inherent Features of hiPSC-Derived Cardiomyocytes. Stem Cell Rep. *10*, 822–833. https://doi.org/10.1016/j.stemcr.2018.01.012.

Ismaili, D., Geelhoed, B., and Christ, T. (2020). Ca2+ currents in cardiomyocytes: How to improve interpretation of patch clamp data? Prog. Biophys. Mol. Biol. *157*, 33–39. https://doi.org/10.1016/j.pbiomolbio.2020.05.003.

Lagrutta, A., Wang, J., Fermini, B., and Salata, J.J. (2006). Novel, potent inhibitors of human Kv1.5 K+ channels and ultrarapidly activating delayed rectifier potassium current. J. Pharmacol. Exp. Ther. *317*, 1054–1063. https://doi.org/10.1124/jpet.106.101162.

Laksman, Z., Wauchop, M., Lin, E., Protze, S., Lee, J., Yang, W., Izaddoustdar, F., Shafaattalab, S., Gepstein, L., Tibbits, G.F., et al. (2017). Modeling Atrial Fibrillation using Human Embryonic Stem Cell-Derived Atrial Tissue. Sci. Rep. *7*, 5268. https://doi.org/10.1038/s41598-017-05652-y.

Lee, J.H., Protze, S.I., Laksman, Z., Backx, P.H., and Keller, G.M. (2017). Human Pluripotent Stem Cell-Derived Atrial and Ventricular Cardiomyocytes Develop from Distinct Mesoderm Populations. Cell Stem Cell *21*, 179–194.e4. https://doi.org/10.1016/j.stem.2017.07.003.

Lemme, M., Ulmer, B.M., Lemoine, M.D., Zech, A.T.L., Flenner, F., Ravens, U., Reichenspurner, H., Rol-Garcia, M., Smith, G., Hansen, A., et al. (2018). Atrial-like Engineered Heart Tissue: An In Vitro Model of the Human Atrium. Stem Cell Rep. *11*, 1378–1390. https://doi.org/10.1016/j.stemcr.2018.10.008.

Lemoine, M.D., Krause, T., Koivumäki, J.T., Prondzynski, M., Schulze, M.L., Girdauskas, E., Willems, S., Hansen, A., Eschenhagen, T., and Christ, T. (2018). Human Induced Pluripotent Stem Cell-Derived Engineered Heart Tissue as a Sensitive Test System for QT Prolongation and Arrhythmic Triggers. Circ. Arrhythmia Electrophysiol. *11*, 1–15. https://doi.org/10.1161/CIRCEP.117.006035.

Loose, S., Mueller, J., Wettwer, E., Knaut, M., Ford, J., Milnes, J., and Ravens, U. (2014). Effects of IKur blocker MK-0448 on human right atrial action potentials from patients in sinus rhythm and in permanent atrial fibrillation. Front. Pharmacol. *5*, 26. https://doi.org/10.3389/fphar.2014.00026.

Mahady, G.B., and Beecher, C.W. (1996). Induction of benzo[c] phenanthridine alkaloid biosynthesis in suspension cell cultures of Sanguinaria canadensis by retinoic acid derivatives. Nat. Prod. Lett. *8*, 173–180. https://doi.org/10.1080/10575639608044891.

Morgenstern, J., Fleming, T., Kliemank, E., Brune, M., Nawroth, P., and Fischer, A. (2021). Quantification of all-trans retinoic acid by liquid chromatography–tandem mass spectrometry and association with lipid profile in patients with type 2 diabetes. Metabolites *11*, 60. https://doi.org/10.3390/metabo11010060.

Pei, F., Jiang, J., Bai, S., Cao, H., Tian, L., Zhao, Y., Yang, C., Dong, H., and Ma, Y. (2017). Chemical-defined and albumin-free generation of human atrial and ventricular myocytes from human pluripotent stem cells. Stem Cell Res. *19*, 94–103. https://doi.org/10.1016/j.scr.2017.01.006.

Rajamani, S., Anderson, C.L., Valdivia, C.R., Eckhardt, L.L., Foell, J.D., Robertson, G.A., Kamp, T.J., Makielski, J.C., Anson, B.D., and January, C.T. (2006). Specific serine proteases selectively damage KCNH2 (hERG1) potassium channels and IKr. Am. J. Physiol. Heart Circ. Physiol. *290*, 1278–1288. https://doi.org/10.1152/ajpheart.00777.2005.

Ravens, U., and Wettwer, E. (2011). Ultra-rapid delayed rectifier channels: Molecular basis and therapeutic implications. Cardiovasc. Res. *89*, 776–785. https://doi.org/10.1093/cvr/cvq398.

Schulz, C., Lemoine, M.D., Mearini, G., Koivumäki, J., Sani, J., Schwedhelm, E., Kirchhof, P., Ghalawinji, A., Stoll, M., Hansen, A., et al. (2023). PITX2 Knockout Induces Key Findings of Electrical Remodeling as Seen in Persistent Atrial Fibrillation. Circ. Arrhythm. Electrophysiol. *16*, e011602. https://doi.org/10.1161/CIRCEP.122.011602.

Sigma. (1996). All Trans-RETINOIC ACID Sigma Prod . No . R 2625.

Soepriatna, A.H., Kim, T.Y., Daley, M.C., Song, E., Choi, B.R., and Coulombe, K.L.K. (2021). Human Atrial Cardiac Microtissues for Chamber-Specific Arrhythmic Risk Assessment. Cell. Mol. Bioeng. *14*, 441–457. https://doi.org/10.1007/s12195-021-00703-x.

Verkerk, A.O., Marchal, G.A., Zegers, J.G., Kawasaki, M., Driessen, A.H.G., Remme, C.A., de Groot, J.R., and Wilders, R. (2021). Patch-Clamp Recordings of Action Potentials From Human Atrial Myocytes: Optimization Through Dynamic Clamp. Front. Pharmacol. *12*, 649414–649416. https://doi.org/10.3389/fphar.2021.649414.

Wettwer, E., Hála, O., Christ, T., Heubach, J.F., Dobrev, D., Knaut, M., Varró, A., and Ravens, U. (2004). Role of IKur in controlling action potential shape and contractility in the human atrium: Influence of chronic atrial fibrillation. Circulation *110*, 2299–2306. https://doi.org/10.1161/01.CIR.0000145155.60288.71.

Wettwer, E., Christ, T., Endig, S., Rozmaritsa, N., Matschke, K., Lynch, J.J., Pourrier, M., Gibson, J.K., Fedida, D., Knaut, M., and Ravens, U. (2013). The new antiarrhythmic drug vernakalant: Ex vivo study of human atrial tissue from sinus rhythm and chronic atrial fibrillation. Cardiovasc. Res. *98*, 145–154. https://doi.org/10.1093/cvr/cvt006.

Wijffels, M.C., Kirchhof, C.J., Dorland, R., and Allessie, M.A. (1995). Atrial fibrillation begets atrial fibrillation: A study in awake chronically instrumented goats. Circulation *92*, 1954–1968. https://doi.org/10.1161/01.CIR.92.7.1954.

Zhang, Q., Jiang, J., Han, P., Yuan, Q., Zhang, J., Zhang, X., Xu, Y., Cao, H., Meng, Q., Chen, L., et al. (2011). Direct differentiation of atrial and ventricular myocytes from human embryonic stem cells by alternating retinoid signals. Cell Res. *21*, 579–587. https://doi.org/10.1038/cr.2010.163.

Stem Cell Reports, Volume *18*

Supplemental Information

A critical role of retinoic acid concentration for the induction of a fully human-like atrial action potential phenotype in hiPSC-CM

Carl Schulz, Muhammed Sönmez, Julia Krause, Edzard Schwedhelm, Pan Bangfen, Dzenefa Alihodzic, Arne Hansen, Thomas Eschenhagen, and Torsten Christ

ERC	[RA] (µM)	BR (bpm)	MDP (mV)	TOP (mV)	APD_{20} (ms)	APD_{90} (ms)	APD_{90-20} /APD_{90}
001	**0**	54±11.5	-78.1±0.9	-77.7±2.6	130.2±19.2	267±33.6	0.54±0.1
	0.01	131.1±14.7 *	-76.6±3.8	-76.4±4.3	86.4±7.9 *	206±16 *	0.58±0.1
	0.1	187.5±68.7 #	-71.8±4.9	-71.3±4.2 #	76.3±11.4	161±26 #	0.53±0
	1	147±36 §	-68.6±0.7 §	-67.7±1.4	8.8±3.6 §	140±25.5	0.92±0 §
021	**0**	74.5±12.3	-74.1±2.1	-74±4.2	108.3±6.9	239±28.1	0.54±0
	0.01	77.2±32.5 *	-67.4±1.1 *	-65.3±4.1 *	114.7±46 *	212±76.1 *	0.39±0.2
	0.1	111±18.4 #	-64.3±2.1 #	-63.9±4.1	70.5±39.3 #	166±39.3 #	0.6±0.1#
	1	125.9±16.7 §	-65.3±4.9	-65±2	17.4±1.6 §	125±32.3 §	0.85±0 §

Supplement Table S1: Effects of different concentrations of retinoic acid (RA) on AP parameters. Mean values±SD for beating rate (BR), maximum diastolic potential (MDP), take-off potential (TOP), action potential duration at 20% (APD_{20}) and 90% repolarization (APD_{90}) and repolarization fraction (APD_{90-20} /APD_{90}) measured in intact EHT based on hiPSC-CM differentiated with different retinoic acid (RA) concentrations. * indicates p<0.05 vs. "0" RA, # indicates p<0.05 vs. 0.01 µM RA and § indicates p<0.05 vs. 0.1 µM RA (ANOVA, same n numbers as in Figure 2).

ERC	[RA] (µM)	ΔAPD_{20}	ΔAPD_{90}	$\Delta V_{Plateau}$
001	**0**	1.5±2	4.2±5.9	3.2±2.1
	0.01	18±14.1 *	27.3±12.4 *	2.3±5.7
	0.1	8.9±12.6	18.1±20.6	1.1±8.9 #
	1	20.26±5.6	-25.8±25.9 §	12±1.7 §
021	**0**	1.8±19.9	9±15	-0.3±.6
	0.01	16.3±8.2 *	24±12.4 *	3.1±14.3
	0.1	6.3±6.2	12.4±11.8	7.5±2.5
	1	18±7.8	-17.3±10 §	13.6±5.1 §

Supplement Table S2: Effects of different concentrations of retinoic acid (RA) on 4-amniopyridine effects. Mean values±SD for the effects of 50 µM 4-aminopyridine (4-AP, expressed as Δ-values) on action potential duration at 20% repolarization (APD_{20}), plateau voltage ($V_{Plateau}$) and action potential duration at 90% repolarization (APD_{90}) measured in intact EHT based on hiPSC-CM differentiated with different retinoic acid (RA) concentrations. * indicates p<0.05 vs. "0" RA, # indicates p<0.05 vs. 0.01 µM RA and § indicates p<0.05 vs. 0.1 µM RA (ANOVA, same n numbers as in Figure S3).

ERC	[RA] (µM)	ΔAPD$_{90}$	ΔTOP	ΔBR
001	**0**	3.1±4.2	0.1±2	3.3±4.3
	0.01	4.3±8.4 *	-0.03±1.4	-8.8±16 *
	0.1	0.1±9.3	-3.6±5.4	-15.9±25.3
	1	-57.1±33 §	-7.2±3.4	-45.6±28.1
021	**0**	4.1±30.7	0.1±1.1	-3.6±12.4
	0.01	-38.2±16.9 *	-1±2.1	-24.4±10.7 *
	0.1	-32±12.2	-1.2±3.3	-40.6±24
	1	-40±7.7 §	-7.8±2.3 §	-61.6±9.8 §

Supplement Table S3: Effects of different concentrations of retinoic acid (RA) on carbachol effects. Mean values±SD for the effects of 10 µM carbachol (CCh, expressed as Δ-values) on action potential duration at 20% repolarization (APD_{20}), take-off potential (TOP) and beating rate (BR) measured in intact EHT based on hiPSC-CM differentiated with different retinoic acid (RA) concentrations. * indicates $p<0.05$ vs. "0" RA, # indicates $p<0.05$ vs. 0.01 µM RA and § indicates $p<0.05$ vs. 0.1 µM RA (ANOVA, same n numbers as in Figure S4).

	Filtropur S® (n=9)	Millex-GP® (n=9)	Whatman® REZIST (n=9)
Recovery in %	29.8±2.4	28.6±7.6	0.1±0.01

Supplement Table S4: Loss of RA by sterile filtration
Mean values±SD for recovery rate of RA concentration in % of unfiltered controls (n=6, data not shown) for three different filters.

Cell type	Adult atrial tissue	**hiPSC-CM**	hiPSC-CM	hESC-CM	hiPSC-CM	hiPSC-CM	hESC-CM	hESC-CM	hiPSC-CM
Culture format	-	**3D**	3D	2D	2D	3D	2D	2D	3D
RA concentration (µM)	-	**1**	1 (?)	1	2	0.25-0.5	1	1	1
Recording technique	Sharp ME	**Sharp ME**	Sharp ME	Patch clamp	Patch clamp	Patch clamp	Patch clamp	Patch clamp	Voltage dye
Temperature	37 °C	**37 °C**	37 °C	36 °C	RT	31 °C	RT	RT	RT
MDP/RMP (mV)	-76	**-68**	-69	-72	-55	-63	-56	-56	n. d.
APA (mV)	105	**82**	80	80	85	n. d.	80	82	n. d.
APD_{20} (ms)	8	**10**	31	21	13*	115*	37*	n. d.	n. d.
APD_{90} (ms)	314	**140**	220	145	189	205	247	169	n. d.
APD_{20}/APD_{90}	0.02	**0.07**	0.14	0.14	0.07	0.56*	0.14	n. d.	0.12*
dV/dt_{max} (V/s)	219#	**104**	95	26	68	7	63	13	n. d.
$V_{Plateau}$	-16#	**-16**	n. d.	-10	n.d.	n. d.	n. d.	n.d.	n. d.
4-AP effect									
APD_{20} (% of baseline)	194	**300**	106	205	n. d.	n. d.	n. d.	n. d.	n. d.
APD_{90} (% of baseline)	88	**81**	100	120	n. d.	n. d.	n. d.	n. d.	n. d.
CCh effect									
APD_{90} (% of baseline)	55	60	82	97	n. d.	69	n. d.	n. d.	n. d.
MDP/RMP (% of baseline)	102	**110**	107	107	n. d.	n. d.	n. d.	n. d.	n. d.
Author/Year	Lemme 2018 Wettwer 2004	**This study**	Lemme 2018	Devalla 2015	Lee 2017	Goldfracht 2020	Laksman 2017	Zhang 2011	Cyganek 2018

Supplement Table S5: Action potential parameters in different types of atrial cardiomyocytes.
Overview about action potential (AP) parameters of different cell types and different studies. The different cell types included adult atrial tissue, cardiomyocytes differentiated from human induced pluripotent stem cells (hiPSC-CM) and cardiomyocytes differentiated from human embryonic stem cells (hESC-CM). The effects of carbachol (CCh) and 4-aminopyridine (4-AP) are given as percentage of baseline values. * indicates an estimated parameter from AP shape.

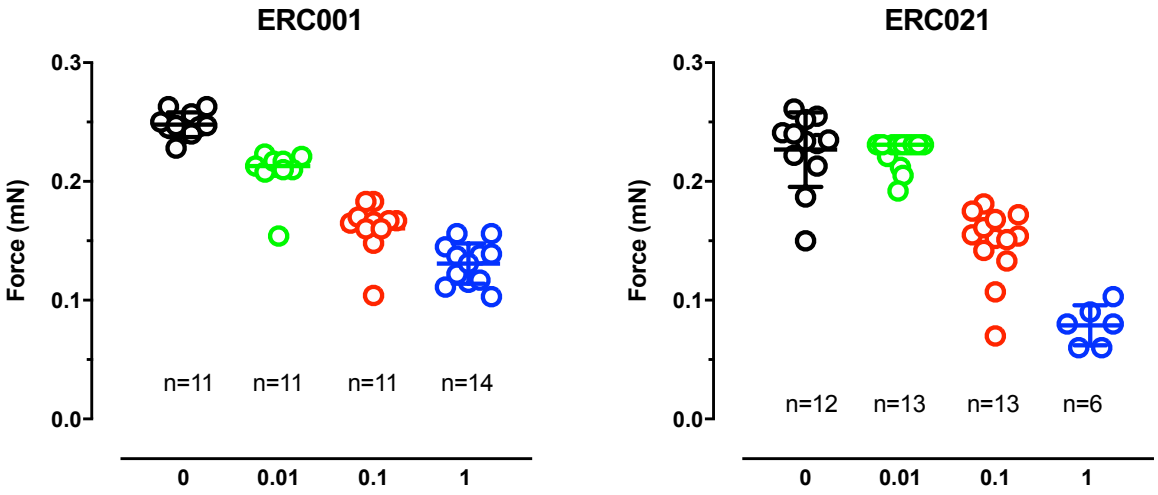

Supplement Figure S1

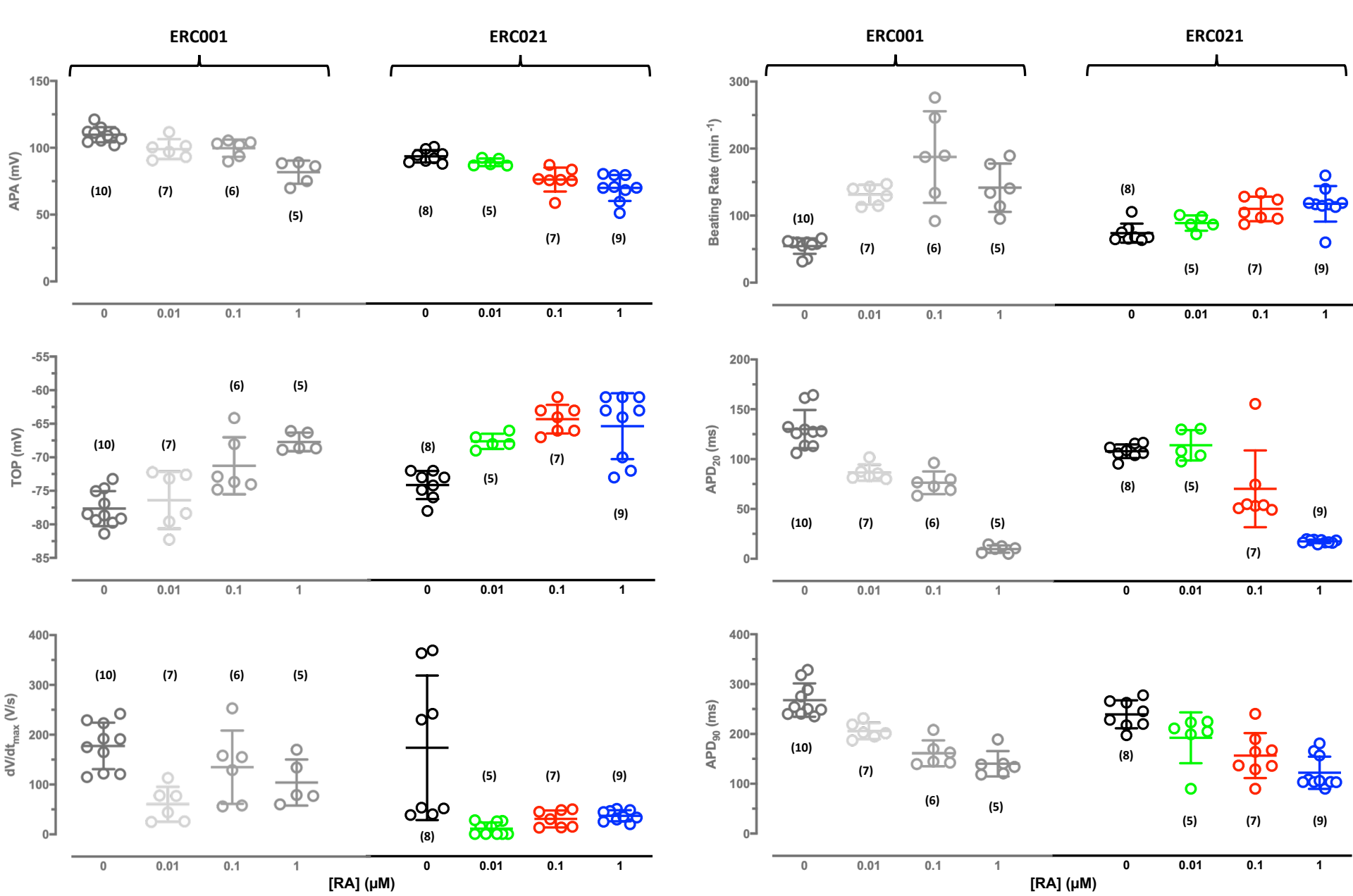

Supplement Figure S2

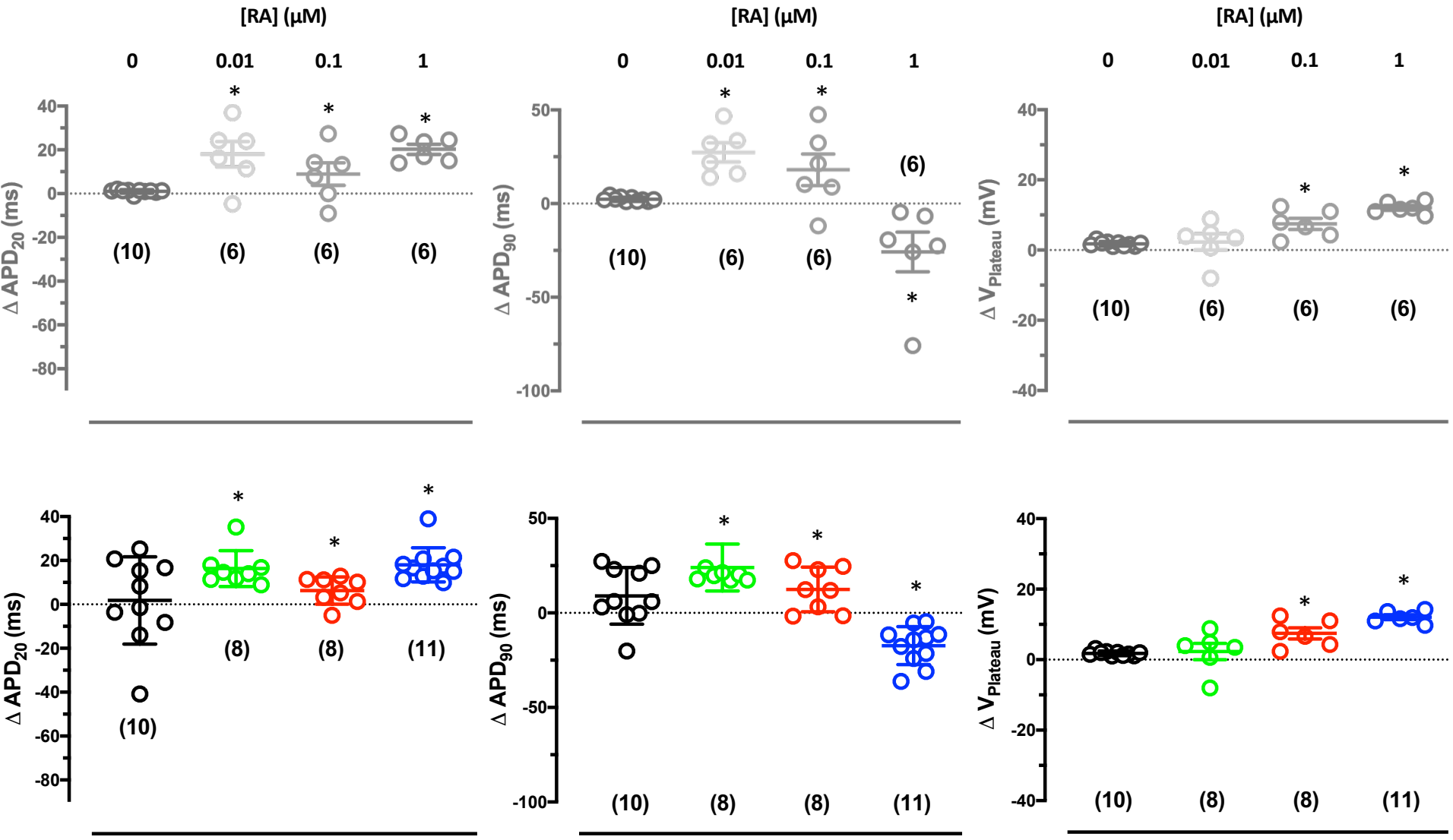

Supplement Figure S3

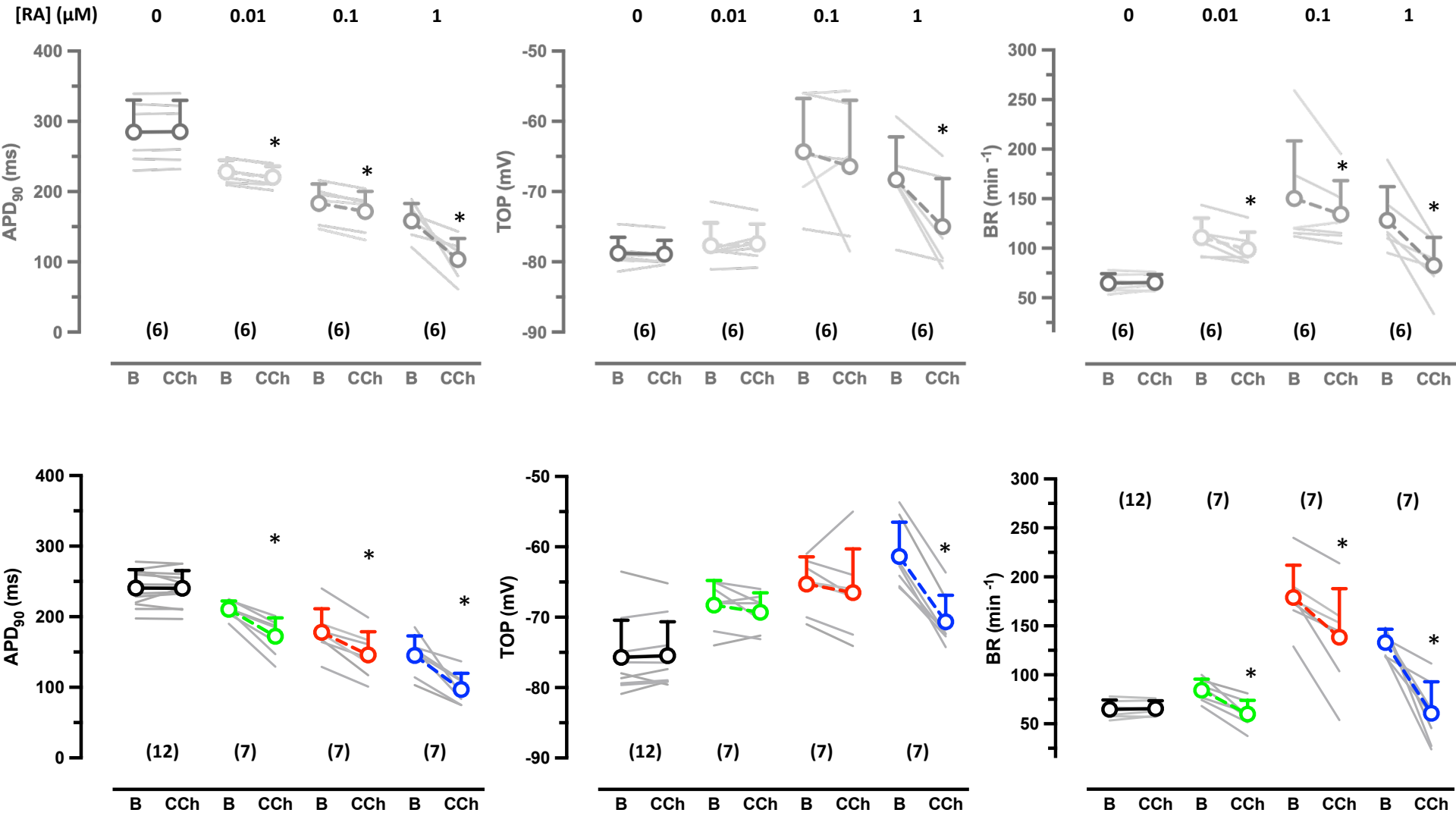

Supplement Figure S4

Legends to supplement figures

Figure S1: Concentration-dependency of RA on force in EHT

Mean values±SD force in EHT from ERC001 and ERC021.

Figure S2: Concentration-dependency of RA on AP in EHT in a second cell line (ERC021)

Summary of results: Mean values±SD for beating rate (**BR**), take-off potential (**TOP**), action potential duration (at 20 and 90% repolarization, **APD_{20}** and **APD_{90}**) and repolarization fraction (**APD_{90}-APD_{50}/APD_{90}**) in EHT from ERC021. * indicates $p<0.05$ vs. 0 RA, one way ANOVA of log transformed data. Number of EHTs resulting from one differentiation run is given in brackets. For better comparison, data for ERC001 (given already in the main manuscript as **Figure 2)** are plotted again in grey.

Figure S3: Concentration-dependency of RA on the AP-response to I_{Kur} block

Top: Data for ERC001 (given already in the main manuscript as **Figure 3)** are plotted in grey. **Bottom:** Data for ERC021. Summary of results for the effects of 4-AP on APD_{20} (**left**), on plateau voltage ($V_{Plateau}$, **middle**) and on APD_{90} in ERC021 (**right**). Open circles indicate mean values±SD. Numbers in brackets indicate number of EHTs resulting from one differentiation run. * indicates $p<0.05$ vs. 0 RA, one-way ANOVA of log transformed data.

Figure S4: Concentration-dependency of RA on carbachol effects on APD_{90} in EHT

Top: Data for ERC001 (given already in the main manuscript as **Figure 5)** are plotted in grey. **Bottom:** Data for ERC021. Summary of results for the effects of CCh on beating rate (BR**, left**), take-off potential (TOP, **middle**) and APD_{90} (**right**). Gray lines indicate individual EHT. Numbers in brackets indicate number of EHTs resulting from one differentiation run. Open circles indicate mean values±SD. * indicates $p<0.05$ vs. basal (paired t-test). Number of EHTs is given in brackets.